The Cryosphere Discuss., 8, 3297–3333, 2014
www.the-cryosphere-discuss.net/8/3297/2014/
doi:10.5194/tcd-8-3297-2014

The Cryosphere Discussions
Open Access

Spatially continuous mapping of snow depth in high alpine catchments using digital photogrammetry

Y. Bühler[1], M. Marty[2], L. Egli[1,3], J. Veitinger[1,4], T. Jonas[1], P. Thee[2], and C. Ginzler[2]

[1]WSL Institute for Snow and Avalanche Research SLF, Davos, Switzerland
[2]Swiss Federal Institute for Forest, Snow and Landscape Research WSL, Birmensdorf, Switzerland
[3]Physikalisch-Meteorologisches Observatorium Davos, World Radiation Center (PMOD/WRC), Davos Dorf, Switzerland
[4]Department of Geography, University of Zurich, Zurich, Switzerland

Received: 3 June 2014 – Accepted: 9 June 2014 – Published: 23 June 2014

Correspondence to: Y. Bühler (buehler@slf.ch)

Published by Copernicus Publications on behalf of the European Geosciences Union.

Spatially continuous mapping of snow depth in high alpine catchments

Y. Bühler et al.

Abstract

Information on snow depth and its spatial distribution is crucial for many applications in snow and avalanche research as well as in hydrology and ecology. Today snow depth distributions are usually estimated using point measurements performed by automated weather stations and observers in the field combined with interpolation algorithms. However, these methodologies are not able to capture the high spatial variability of the snow depth distribution present in alpine terrain. Continuous and accurate snow depth mapping has been done using laser scanning but this method can only cover limited areas and is expensive. We use the airborne ADS80 opto-electronic scanner with 0.25 m spatial resolution to derive digital surface models (DSMs) of winter and summer terrains in the neighborhood of Davos, Switzerland. The DSMs are generated using photogrammetric image correlation techniques based on the multispectral nadir and backward looking sensor data. We compare these products with the following independent datasets acquired simultaneously: (a) manually measured snow depth plots (b) differential Global Navigation Satellite System (dGNSS) points (c) Terrestrial Laser Scanning (TLS) and (d) Ground Penetrating Radar (GPR) datasets, to assess the accuracy of the photogrammetric products. The results of this investigation demonstrate the potential of optical scanners for wide-area, continuous and high spatial resolution snow-depth mapping over alpine catchments above tree line.

1 Introduction

Snow is an important resource in alpine regions not only for tourism (e.g. Elsasser and Bürki, 2002; Nöthiger and Elsasser, 2004; Rixen et al., 2011) but also for hydropower generation and water supply (e.g. Marty, 2008; Farinotti et al., 2012), ecological aspects of the local mountain flora and fauna (e.g. Wipf et al., 2009) and natural hazard prevention, such as flood forecast in spring and early summer for the valleys downstream. For the latter it has been shown that the snow distribution at the winter maximum before the beginning of the melting period strongly determines the temporal evolution of the remaining snow resources and – if converted to snow water equivalent (Jonas et al., 2010) – the potential melt water run-off during the melting period (Egli et al., 2012). Several studies reported a very high spatial variability of snow depth and other snow pack parameters at different spatial scales in mountainous regions. (e.g. Elder et al., 1991; Schweizer et al., 2008; Lehning et al., 2008; Grünewald et al., 2010; Egli, 2011). This high variation of snow cover distribution at already very small scales requires a high spatial resolution of snow samples to measure different parameters of the snow pack such as e.g. the areal mean snow depth on complex Alpine topography and the temporal evolution of snow covered areas during melt with high areal representativeness and low absolute uncertainty. In other words, snow pack monitoring in Alpine terrain requires an area wide observation with a large number of snow depth point measurements distributed over the area of interest.

Currently, in the Swiss Alpine region snow depth is measured at specific locations by automated weather stations or observers in the field, while both observations are restricted to flat sites exhibiting a rather homogeneous snow cover (Bründl et al., 2004; Egli, 2008). These flat field point measurements are assumed to represent snow cover characteristics for a larger area around the stations and are therefore interpolated over large distances and are combined with snow cover information from optical satellites (Foppa et al., 2007). This method is unable to capture the small-scale variability of snow depth. Investigations on the representativeness of point snow depth measurements on snow depth for entire catchments are lacking. Terrestrial Laserscanning (TLS) was previously used to derive spatially continuous snow depth (Prokop, 2008; Grünewald et al., 2010). Even though the accuracy of such measurements is very good (usually better than 0.1 m, depending on laser footprint and distance from sensor), large-scale catchments such as the Dischma valley (Fig. 1) cannot be covered completely. Data acquisition with TLS is time/manpower consuming and only possible at easily accessible spots under fair conditions (avalanche situation, weather) for areas within line-of-sight from the measurement location. This results in limited coverage and many data gaps e.g. behind bumps. Airborne laser scanning (ALS) from helicopters or airplanes can cover larger areas in shorter time also under difficult avalanche danger situations. Recent studies demonstrate that accurate mapping of snow depth is possible (Deems et al., 2013; Mevold and Skaugen, 2013). However, the costs to cover larger areas are very high (Bühler et al., 2012) and over-flights are also restricted to fair weather conditions.

Remote sensing instruments have been used for snow related studies since such data was available (e.g. Rango and Itten, 1976; Dozier, 1984; Hall and Martinec, 1985). A very common parameter measured by remote sensing instruments is snow-covered area (SCA). Operational products on global scale such as MODIS Snow-cover Products (Hall et al., 2002) or GlobSnow (Koetz et al., 2008) are widely used today (Frei et al., 2012). For example Dozier (1989), Nolin and Dozier (1993), Fily et al. (1997) and Dozier et al. (2009) published investigations on snow grain size with finer spatial resolution. Snow depth and Snow water equivalent (SWE) has been assessed using passive microwave sensors (e.g. Ulaby and Stiles, 1980; Chang et al., 1982; Pulliainen, 2006). However due to the coarse spatial resolution of these sensors (25 km), the results do not display small-scale snow cover characteristics of alpine catchments. Active microwave sensors use much smaller wavelength (mm to cm) and achieve finer spatial resolutions up to 20 m (e.g. Schanda et al., 1983; Shi and Dozier, 2000; Rott and Nagler, 1994). However this method is limited for dry snowpacks and faces problems in steep high-alpine terrain (Buchroithner, 1995). Nolin (2011) and Dietz et al. (2012) give an overview on recent advances in remote sensing of snow.

In this investigation we propose digital photogrammetry based on high spatial resolution aerial imagery (0.25 m) to calculate digital surface models (DSM) of winter and summer terrain. Traditional photogrammetry using analogue aerial imagery and 8bit digital sensors faced problems over snow-covered areas mainly due to saturation and the homogenous surface (Kraus, 2004). Modern digital sensors can acquire data with 12bit radiometric resolution to overcome these limitations. We calculate spatially continuous snow depth maps using the summer and winter DSMs for two test sites near

Davos, Switzerland (145 km^2 in total). This technology is much more economical to cover large areas than ALS or TLS but still has an acceptable spatial resolution to map the small-scale spatial variability. To assess the accuracy of our results we compare the calculated snow depths to hand measurements, dGNSS points, TLS measurements and GPR transects acquired simultaneously with the aerial imagery.

2 Test sites Wannengrat and Dischma, Davos, Switzerland

The two areas covered by the ADS80 sensor on a Pilatus Porter airplane on 20 March 2012 (winter), 12 August 2010 (summer Wannengrat) and 3 September 2013 (summer Dischma) are located close to the winter sport resort Davos in the eastern part of Switzerland (Fig. 1).

The Wannengrat test site is located in the north of Davos and covers an area of approximately 3.5 km × 7.5 km (26.25 km^2). The valley bottom is about 1500 m a.s.l., the highest peaks reach up to 2780 m a.s.l. (Amselflue at the southwestern part of the test site). The large ski resort Davos–Parsenn is located at the northeastern edge of the test site. The covered mountain chain is characterized by high-alpine meadows, rock faces and scree covered areas. The area below 2000 m a.s.l. is covered by sparse- and from ca. 1800 m a.s.l. by dense forest. The Wannengrat area works as test site for various research project at the WSL Institute for Snow and Avalanche research SLF mainly because of the very good accessibility from Davos even if the avalanche danger level is considerable. We collected hand measured snow depth plots, dGNSS points and TLS datasets close to the Wannengrat peak as reference datasets (see chapter 3.2) at the day of the ADS80 data acquisition.

The Dischma test site is a high-alpine valley branching from the main valley of Davos (1500 m a.s.l.) in southeastern direction up to 2000 m a.s.l. at the end of the valley covering an area of ca. 7 km × 17 km (119 km^2) containing the complete catchment of the Dischma creek where different hydrological studies are performed (Bavay et al., 2009). The peaks surrounding this catchment reach up to 3130 m a.s.l. (Piz Grialetsch). Forest

TCD
8, 3297–3333, 2014

is covering the lower part of the valley up to 2000 m a.s.l. The southeastern two thirds of the valley are completely forest free. We collected GPR snow depth measurements at the valley bottom in the northwestern part of the test site as reference data at the day of the ADS80 data acquisition. Because the central flight strip at the valley bottom was corrupted in the summer 2010 dataset, resulting in a low quality summer DSM, we repeated the flight in summer 2013.

3 Sensors and datasets

To measure spatially continuous snow depth and to validate these measurements we use independent state-of-the-art technologies available. It is a difficult task to measure multiple, spatially widely distributed snow depths in high-alpine areas within a short timespan. Several teams have been in the field on the day of the ADS80 data acquisition, guaranteeing a small temporal offset to the ADS80 imagery because snow depth can change very quickly under spring conditions.

3.1 Airborne opto-electronic Scanner ADS80

Two optoelectronic line scanner datasets were acquired with the ADS80 sensor (Fig. 2). The acquisition of the summer images was realized on 12 August 2010 (Wannengrat) and 3 September 2013 (Dischma). Winter imagery of the snow-covered sites was acquired on 20 March 2012 (close to the maximum snow cover, peak of winter). The covered area consists of 12 overlapping image strips (approx. 70 % overlap across track). The mean Ground Sampling Distance (GSD) of the imagery is 0.25 m, limited through the minimal flying height for high alpine terrain (Bühler et al., 2012). The ADS80 scanner acquires simultaneously four spectral bands (red, green, blue, near infrared) and a panchromatic band with a radiometric resolution of 12 bits under multiple viewing angles. GNSS/IMU supported orientation of the image strips supplemented by the use of ground control points achieve a horizontal accuracy (x, y) of 1–2 GSD (0.25–0.5 m).

This sensor was successfully used to detect avalanche deposits in the area of Davos (Bühler et al., 2009). More detailed information on the Leica ADS opto-electronic scanner can be found in Sandau (2010). By end of 2013 the successor sensor ADS100 gets available. This sensor holds twice as many pixels than the ADS80 sensor, resulting in a doubled spatial resolution (12.5 cm) for the same flying height above ground.

3.2 Reference datasets

3.2.1 Manual snow depth measurements

Simultaneous with the ADS80 data acquisition, a field team acquired manual snow depth measurements using a 3.2 m avalanche probe at 15 different plot locations within the test site Wannengrat. A plot consists of 5 by 5 probe measurements with a distance of 2 m in between (Fig. 3) resulting in 375 single probe measurements localized using dGNSS of the corner points. Because snow depth can vary substantially within the distance of some decimeters if there is e.g. a rock at the surface (Lopez-Moreno et al., 2006), we use the average snow depth and the standard deviation to compare it to the corresponding ADS80 snow depth values within this 10 by 10 m area. The acquisition of field measurements is very challenging because the terrain is steep and the human mobility is limited. The avalanche danger for wet snow avalanches rises quickly during the day sunny spring weather conditions, limiting the time the field team can move within the test sites. Therefore the number of performed field measurements at 15 plots distributed over an area of 1 by 1.5 km is close to the possible maximum. Because this number is not sufficient to assess the potential of the proposed method, we apply further reference data sets.

3.2.2 Differential Global Navigation Satellit System (dGNSS) measurements

During ADS80 data acquisition on 20 March 2012, 137 dGNSS points were measured with the Leica GPS 1200 device in the test site Wannengrat (Fig. 4). The points were

TCD
8, 3297–3333, 2014

measured real-time using the virtual reference station of the swisstopo AGNES network. The surveyed points show a horizontal accuracy better than 1 cm (1 stdev) and a vertical accuracy better than 2 cm (1 stdev) respectively. Measured points represent the top of the snow cover in m a.s.l.

3.2.3 Terrestrial Laserscanning (TLS)

In the last decade, terrestrial laser scanning has been increasingly applied for continuous snow depth mapping (e.g. Veitinger et al., 2014; Deems et al., 2013; Prokop 2008). To calculate snow depth, an elevation model of the bare ground and another one of the snow covered winter surface is produced. Snow depth is then obtained by subtracting the two surfaces from each other. In this study we use the Riegl LPM-321 device operating at 905 nm. This device proofed to accurately measure snow depth in alpine terrain (Prokop, 2008). Grünewald et al., 2010, comparing TLS measurements to Tachymeter measurements, reported a mean vertical deviation of 4 cm with a standard deviation of 5 cm at a distance of 250 m using the LPM-321. To assure the quality of the laser scans, we additionally performed reproducibility tests. A laser scan acquired in a coarse resolution (< 15 min) was compared with the full resolution acquisition. This allows detecting misalignments between the two datasets due to an instable scan setup (unstable tripod, wind influence, etc). Scans which showed a mean difference larger than 10 cm were excluded. The upper end of the Steintaelli was scanned once in summer 2011 and a second time on 20 March 2012 during the ADS80 data acquisition (Fig. 5). Fix installed reflector points were used to match the summer and winter TLS datasets.

3.2.4 Ground Penetrating Radar (GPR)

GPR data were collected using a MALÅ ProEx system configured for synchronous measurements with four pairs of separable shielded 400 MHz antennas. The antennas were set up as a common-mid-point (CMP) array with separation distances of 0.31, 0.95, 1.6, and 2.8 m respectively. The GPR antennas were mounted on two pulkas, which were rigidly connected to one another to guarantee fix relative antenna positions throughout the measurements. This assembly was pulled along a transect of 4.8 km length. After initial stacking of four individual traces, data were recorded every 0.5 s, which resulted on average in one record every 30 centimeters along the transect. GPS coordinates were taken every second along the transect using an onboard GPS receiver as well as an external Trimbel GeoExplorer 6000 DGPS system. GPS data were slightly smoothed before associating them with the GPR data records. Snow depth data were obtained using standard CMP analysis procedures partly involving the commercial software package ReflexW 7.0 (Sandmeier, 2013). Along the GPR transect we obtained 130 manual snow depth readings. These data were used for cross validation of the GPR data. Concurrent GPR and manual data ranged in snow depth from 0.76 to 2.70 m. Correlation between both data sets resulted in an R^2 of 0.96 and a RMSE of 0.07 m.

4 Generation of summer and winter digital surface models

For DSM generation we use the "Adaptive Automatic Terrain Extraction" (ATE) as part of the SOCETSET software version 5.4.1 from BAE SYSTEMS. The software is based on an area-based algorithm calculating similarity measures with a two-dimensional cross-correlation approach. ATE has no need for user input on specific image matching strategies and parameters as a function of terrain type. ATE uses an "inference engine" which adaptively generates image matching parameters depending on facts such as terrain type, signal power, flying height or X and Y parallax. A user given post spacing distance is used to control image correlation spacing (e.g. 2 m), hence cross correlation is not calculated for every image pixel (Zhang and Miller, 1997).

As this study focuses on Snow depth mapping for wide scale applications, we set the spatial resolution of the derived DSM to 8*GSD (8*0.25 m), which shows significantly lower demand in CPU usage compared to a resolution of 1 m. Additionally we apply

TCD
8, 3297–3333, 2014
Spatially continuous mapping of snow depth in high alpine catchments
Y. Bühler et al.

a 3*3 low pass filter to adapt the final products to the continuous nature of snow-covered areas.

In our research setup, single buildings and forest/scrub cannot be modeled with sufficient horizontal accuracy due to the limited spatial resolution of the input imagery. Slight differences in x, y positions of such objects in the summer and winter DSM would lead to big outliers in the snow depth product. Therefore all buildings and forest/scrub areas were masked out. For the detection of forest/scrub areas a combination of NDVI (Normalized Differenced Vegetation Index) and a canopy height layer was applied. With this approach, all visible vegetation in the winter images and vegetation higher than 1.5 m in the summer images were masked out. The detection of buildings (settlements) only from spectral or elevation information is not feasible since rock covered areas return an identical spectral signature than settlements and are prone to big outliers. Therefore we use the building layer from the Topographic Landscape Model (TLM) of the Swiss Federal Office of Topography. This step might not be necessary if the input imagery would have a higher spatial resolution (15 cm or better).

Large-scale imagery of a mountainous, snow covered landscapes show a maximal range of radiometric image information over little distance, which is highly demanding for image correlation processes. For this reason generating a complete DSM from one entire image strip is not expected to give optimal results for snow covered areas. As a response to this challenge we divided the test site in 809 tiles for which DSMs were calculated separately. Another well-known issue in steep mountain areas is a not optimal viewing angle or even occlusion in an image strip. Considering this difficulty, we calculated two DSMs for each tile, using the "most nadir" and the "second most nadir" – CIR image strips (near infrared, red, green) to increase the chance of a good image match for a given point on the ground. For the generation of the final DSM we calculated the mean slope for every processed DSM-tile. By selecting the DSM with the smaller mean slope for every given tile, big blunders caused by a not optimal viewing angle or occlusion could mostly be automatically eliminated. We used the described approach to process all DSMs.

TCD
8, 3297–3333, 2014

Orientation of ADS80 image strips has to be considered as a critical point especially for winter images. All processing and evaluation efforts are worthless if there is a lack of accuracy in image orientation. Due to a small number of highly accurate reference points in remote areas and sometimes almost unrecognizable ground control points in snow covered, high alpine regions (e.g. east part of Dischma valley without any anthropogenic features) orientation quality shows certain limitations. For the mentioned areas, orientation during the post processing of image strips (software Leica xPro) could not be substantially improved, resulting in a final orientation accuracy of about 1 GSD. Well distributed artificial reference points measured at the ground with dGNSS could improve the orientation quality substantially but were not available for the winter 2012 imagery.

5 Results and validation

To quantify the accuracy of the digital photogrammetry products, we use the following measures recommended by Höhle and Höhle (2009) to compare elevation datasets from different sources:

(a) The root mean square error

$$\mathrm{RMSE} = \sqrt{\frac{1}{n}\sum_{i=1}^{n}\Delta h_i^2} \quad (1)$$

this measure is often used and simple to calculate but very prone to outliers.

(b) Normalized median absolute deviation

$$\mathrm{NMAD} = 1.4826 \cdot \mathrm{median}_i(|\Delta h_i - m_{\Delta h}|) \quad (2)$$

where Δh_i denotes the individual errors and $m_{\Delta h}$ is the median of the errors.

TCD
8, 3297–3333, 2014

(c) Additionally we use the empirical correlation coefficient

$$\text{corr}_e = \frac{\sum_{i=1}^{n}(x_i - \bar{x})(y_i - \bar{y})}{\sqrt{\sum_{i=1}^{n}(x_i - \bar{x})^2 \sum_{i=1}^{n}(y_i - \bar{y})^2}} \tag{3}$$

to assess how well two snow depth measurements from different sources correlate.

To make the comparison of elevations in DEM products possible it is crucial that a coherent coordinate system is applied for all datasets. We use the swisstopo LV1903 LN03 system with the elevation reference point at Repere Pierre du Niton H(RPN) = 373.6 m a.s.l. in Genva, Switzerland (swisstopo 2008).

5.1 Photogrammetric summer DSMs (DSM_{ADS})

Three DSM_{ADS} (winter 2012, summer 2010 and 2013) were processed for this study. For a quantification of the quality of the derived DSM_{ADS} we perform an accuracy assessment using an airborne laser scanning dataset (DTM_{ALS}) acquired in summer 2009 as a reference, assuming the changes in terrain to be negligible (which might not be true for areas prone to erosion and deposition). Airborne laser scanning is reported as very accurate method for DTM generation in various studies (e.g. Aguilar and Mills, 2008; Höhle and Höhle, 2009) also on snow (Deems et al., 2013) and in high alpine terrain (Bühler and Graf, 2013). The quantification of the accuracy is described by the distributions of vertical deviations between the two datasets (886 000 points). Vegetation and buildings were excluded for the analysis.

The statistical measures in Table 1 show a good correspondence between the DTM_{ALS} and DSM_{ADS}. The RMSE value without outlier removal indicate the presence of big outliers. Since the mean values of the deviations with and without outlier removal differ only by 3 cm these big outliers are both, negative and positive. A detailed quality assessment on DSMs derived by ADS80 image strips in very steep and complex alpine terrain showed that the accuracy of photogrammetric DSMs decrease significantly in terrain steeper than 50°, explaining the occurrence of the above mentioned outliers (Bühler et al., 2012).

In Fig. 6 on the right image correlation completeness in terms of correlated and interpolated points is shown for a section of testsite Wannengrat for winter 2012. Image matching completeness for the whole test site is given in Table 2 (Wannengrat and Dischma without buildings and vegetation). These results show the high matching success with the 12 bit imagery in particular over snow coverd areas.

5.2 Snow depth maps

The snow depth maps are calculated by subtracting the winter DSM from the summer DSM. Its spatial resolution is 2 m equivalent to the input DSMs. Resulting values higher than 15 m and lower −0.5 m are considered outliers and are masked out. Values between 0 and −0.5 are set to 0 because negative snow depths cannot occur and there is a high probability that there is no or only very few snow at these spots. Consulting the input orthophotos of the winter data acquisitions allows identifying if a certain area is snow free or not. Overall, 19.42 % of all pixels are classified as trees and scrubs and 1.65 % as buildings. From the remaining pixels 3.15 % were classified as outliers and 4.83 % are set to zero.

The generated snow depth maps (Figs. 7. and 8.) reveal a very high spatial variability of snow depth even within small distances. Snow depth can vary by more than 5 m within a few meters. Snow traps for wind-blown snow and deposits from past avalanche events get clearly visible. We identify the same snow trap features in the Wannengrat area, which are reported by Grünewald et al., 2010 measured in winter 2008. This indicates that snow traps and cornices are persistent over different winters due to dominant main wind directions. High snow depth values due to avalanche deposits are persistent in tracks where avalanches occur several times during one winter but are not where avalanches occur with return periods of more than one year.

The large area at the northern edge of the Dischma test site (Fig. 7.) classified as outliers is Lake Davos. This natural lake is used for power generation during winter and the surface level is lowered by up to 50 m. By subtracting the winter DSM from the summer DSM we get clearly negative values in this area, which are classified as outliers. The large outlier areas at the southern edge of the investigation area are glaciers of the Grialetsch range. These small glaciers lost a significant part of their volume between summer 2013 (summer DSM) and winter 2012 (winter DSM) and lowered their surface elevation (Zemp et al., 2006). Therefore highly positive values occur and are classify as outliers. Further outliers occur in very steep terrain (> 50°) because the footprint of the sensors is very small in such areas (Bühler et al., 2012), demonstrating the limitation of the proposed method for snow in rock faces. These areas are less relevant for most snow depth applications because less snow is usually accumulated (e.g. Fischer et al., 2011).

5.3 Snow depth validation using independent reference datasets

5.3.1 Differential Global Navigation Satellite System (dGNSS) measurements

A comparison of the ADS derived Winter 2012 DSM with 137 dGNSS points, describing elevations in m a.s.l. (top of the snow cover) results in a RMSE of 0.37 m and a NAMD of 0.28 m. With a mean of 0.21 m the ADS DSM models the surface of the snow cover systematically higher than dGNSS measurements. For the area shown in Fig. 1 it can therefore be assumed, that snow cover thickness is overestimated using photogrammetric methods, mainly because of orientation inaccuracies. A bias introduced during the dGNSS survey could be caused by the penetration of the dGNSS device into the soft snow cover by a few cm‘s which could explain some of the mean differences in elevation values between photogrammetry and dGNSS measurements.

TCD
8, 3297–3333, 2014

5.3.2 Terrestrial Laserscanning (TLS)

We compare the independently acquired TLS derived snow depth (TLS winter minus TLS summer) with the ADS derived snow depth (Fig. 9). In total we look at 55 272 pixels of 2 m resolution. It is hard to detect differences between the two snow depth products on first shight. All prominent snow features such as filled channels, cornices or blown out areas are clearly visible in both products. In the difference image between the two snow depth products, four regions with large deviations up to 2 m stand out (marked with black circles in Fig. 9c). Three negative deviations (red, TLS higher than ADS) are located in small depressions. In these areas the incident angle of the laser beam is very flat resulting in lower accuracies. The ADS sensor is looking from nadir at these spots, producing more reliable snow depth values. On the ridge at the southern end of the subset a large cornice was formed by wind during the winter (see Fig. 5 in the background). This cornice is mapped with too large snow depth by the ADS dataset because of the nadir-viewing angle. The TLS sensor is seeing the overhanging cornice from below producing better snow depth measurements than the ADS. However the correlation analysis for the two snow depth measurement methods results in cor_e = 0.94, the RMSE is 0.33 m and the NMAD 0.26 m. This proves the quality of the ADS snow depth measurements especially concerning the complex terrain of this subset (mean slope 28°, elevation from 2332 m to 2639 m a.s.l.).

5.3.3 Hand-measure plots

The comparison of the snow depth values derived from the ADS80 DSMs to the manual plot measurements is given in Table 3. In three out of the 15 plots the snow depth exceeds the length of the avalanche probe (3.2 m) and the correct values could not be measured at all 25 points (measurements deeper than 3.2 m: plot1, 14; plot11, 5; plot 13, 5). The hand measurements could also be distorted by not plumb-vertical penetration of the snow cover (especially in deep snow packs), by thick ice layers in the snowpack, which cannot be penetrated by the avalanche probe, by rough bedrock

TCD
8, 3297–3333, 2014

or by inaccuracies of the positioning by dGNSS. Therefore we average the 25 single measurements and compare the mean and standard deviation (std) of an entire plot to the ADS80 DSM based snow depth values (mean of all cells within the plot area).

The RMSE is 0.35 m for the mean snow depth and 0.13 m for the standard deviation over all plots. The NMAD is 0.22 (mean) and 0.06 m (std). The correlation coefficient cor_e for the mean snow depth is 0.92 and 0.81 for the standard deviation. If we eliminate the three plots (1, 11 and 13), which contain unreliable measurements, the RMSE is reduced to 0.19 (mean) and 0.11 (std) and the NMAD to 0.18 m (mean) and 0.06 m (std). The correlation coefficients shift to 0.95 (mean) and 0.76 (std). The standard deviation is underestimated by the DSM_{ADS} derived snow depth values due to the smoothing effect of the 2 m pixel size. However these results indicate the feasibility of the proposed method for snow depth mapping.

5.3.4 Ground Penetrating Radar (GPR)

To allow comparison between GPR snow depth measurements and the ADS measurements, we assigned all individual 18 136 GPR point measurements to the 2 m × 2 m ADS raster, and calculated the mean of all GPR values within each cell, resulting in 1522 cells with GPR-based comparison data. The variability of the GPR snow depth within these cells amounted to between 0.1 and 0.3 m. Parts of the GPR data have been obtained close to taller vegetation such as trees and bushes. However, affected measurements have been masked out before comparison, as ADS data cannot represent snow depth under forest canopy.

Comparing GPR to ADS data results in an overall RMSE of 0.43 m and an NMAD of 0.36 m. This is approx. 0.1 m worse compared to the reference data sets acquired at the Wannengrat area. The overall correlation coefficient between both data sets is 0.45 (Fig. 10a) only, note however that the GPR data set features a significantly lower range in snow depth when compared to the TLS data set (Fig. 9, Table 4). When analyzing different segments of the GPR dataset we find considerable differences. While the correlation is acceptable for individual GPR segments that feature a large snow depth variability (Fig. 10b) it appears less favorable for GPR segments with a small variability in snow depth (Fig. 10c). The inferior comparison of ADS to GPR reference data from the Dischma area can be explained by the greater distance of the ADS sensor to the ground. While the Wannengrat reference data sets have been collected in an altitude of approximately 2400 m a.s.l., the valley ground of the Dischma, where most of the GPR data have been collected, has an elevation of approximately 1600 m a.s.l. This results in a higher effective ground sapling distance (GSD) and therefore in a lower accuracy of the corresponding ADS data data set. This finding indicates that spatial resolution of input imagery matters for the accuracy of the resulting snow depth estimates.

6 Conclusions

The presented results demonstrate the potential of digital photogrammetry for catchment wide snow depth mapping. The extensive validation using independent datasets acquired simultaneously with the aerial-imagery reveals an accuracy of approx. 30 cm (RMSE, NMAD), equivalent to ∼ 1 GSD of the images (Table 4). Due to the high radiometric resolution of the images (12bit) and the use of near infrared bands, the images were not saturated over bright areas and information could be acquired even in cast shadow areas. The image correlations works even in very homogeneous snow covered areas. Table 2 reveals almost the same correlation success with winter images compared to summer images. This antiquates the assumption that photogrammetry is not working on snow. The resulting snow depth maps reveal the high spatial variability of snow depth even within distances of some meters. Snow traps for wind-blown snow, cornices and deposits from past avalanche events can be identified easily by high snow depth values up to 15 m. Compared to airborne laser scanning the proposed method is slightly less accurate but much more economic if large areas have to be covered repeatedly. Furthermore digital photogrammetric DSMs can be generated using unmanned aerial vehicle UAV's flying close to the ground and producing higher spatial resolution imagery (Mancini et al., 2013) resulting in more accurate and much more economic snow depth maps. However, the feasibility of UAVs in high alpine terrain has to be further investigated especially concerning flight-time and strong-wind conditions.

Challenging for image correlation on snow-covered terrain are the big spectral differences of surface cover properties between bright snow-covered slopes and rocky terrain in shadow. If terrain properties change within short distances, the probability of big outliers or even complete failures of image matching rises. We modeled only 1 km^2 per step to decrease these differences within the correlated images. With this approach massive failure of image matching could mostly be averted. For some tiles, issues with big outliers remained, showing a certain limitation to the modeling of snow-covered areas with the used image correlation Software. For future investigations the choice of more advanced image correlation algorithms like methods of the semi-global matching family is expected to solve part of this limitation. The modeling of steep slopes ($> 50°$) using image-matching techniques is not accurate mainly due to the small footprint of the sensor (Bühler et al., 2012). But because snow accumulation is less dominant in such steep slopes (Schweizer et al., 2008; Fischer et al., 2011), these areas are less important for applications in hydrology and avalanche science. The proposed methodology is not working in forested terrain or in regions covered by scrubs. Therefore these areas were masked out prior to the snow map calculation. The accuracies of final DSM products depend heavily on the image strip orientation quality. Here we faced two major limitations: (a) we could gather only a small number of reference points, measured with high accuracy in x, y and z and (b) in areas deeply covered by snow without anthropogenic signs visible, the recognition of clearly identifiable reference points is sometimes almost impossible. Therefore we see big potential to increase the quality of final products by collecting more accurately measured reference points and by signalizing reference points in remote parts of the covered area for upcoming data acquisition campaigns.

Next steps will be to acquire similar datasets at the end of upcoming winters for interannual comparison of snow depth. This would also open the door for investigations on the representativeness of snow depth measurements at given points for example

TCD
8, 3297–3333, 2014

at automated weather stations. Comparisons between snow depth maps generated by LiDAR and digital photogrammetry will provide more information on the specific strengths and weaknesses of the two methodologies.

Acknowledgements. The authors thank Leica Geosystems for the provision of the ADS80 datasets as well as the SLF field teams for helping with the reference data acquisition.

References

Aguilar, F. J. and Mills, J. P.: Accuracy assessment of lidar-derived digital elevation models, Photogramm. Rec., 23, 148–169, 2008.

Bavay, M., Lehning, M., Jonas, T., and Löwe, H.: Simulations of future snow cover and discharge in Alpine headwater catchments, Hydrol. Process., 23, 95–108, 2009.

Bründl, M., Etter, H.-J., Steiniger, M., Klingler, Ch., Rhyner, J., and Ammann, W. J.: IFKIS - a basis for managing avalanche risk in settlements and on roads in Switzerland, Nat. Hazards Earth Syst. Sci., 4, 257–262, doi:10.5194/nhess-4-257-2004, 2004.

Buchroithner, M. F.: Problems of mountain hazard mapping using spaceborne remote sensing techniques, Adv. Space Res., 15, 57–66, 1995.

Bühler, Y., Hüni, A., Christen, M., Meister, R., and Kellenberger, T.: Automated detection and mapping of avalanche deposits using airborne optical remote sensing data, Cold Reg. Sci. Technol., 57, 99–106, 2009.

Bühler, Y., Marty, M., and Ginzler, C.: High resolution DEM generation in high-Alpine terrain using airborne remote sensing techniques, Transactions in GIS, 16, 635–647, 2012.

Bühler, Y. and Graf, C.: Sediment transfer mapping in a high-alpine catchment using airborne LiDA R. in: Graf, C. (Red.) Mattertal – ein Tal in Bewegung. Publikation zur Jahrestagung der Schweizerischen Geomorphologischen Gesellschaft 29 June–1 July 2011, St. Niklaus, Birmensdorf, Eidg. Forschungsanstalt WSL, 113–124, 2013.

Chang, A., Foster, J., Hall, D., Rango, A., and Hartline, B.: Snow water equivalent estimation by microwave radiometry, Cold Reg. Sci. Technol., 5, 259–267, 1982.

Deems, J., Painter, T., and Finnegan, D.: Lidar measurement of snow depth: a review, J. Glaciol., 59, 467–479, 2013.

Dietz, A., Kuenzer, C., Gessner, U., and Dech, S.: Remote sensing of snow – a review of available methods, Int. J. Remote Sens., 33, 4094–4134, 2012.

Dozier, J.: Snow reflectance from landsat-4 thematic mapper, IEEE T. Geosci. Remote, GE-22, 323–328, 1984.
Dozier, J.: Spectral signature of alpine snow cover from the Landsat thematic mapper, Remote Sens. Environ., 28, 9–22, 1989.
Dozier, J., Green, R. O., Nolin, A. W., and Painter, T. H.: Interpretation of snow properties from imaging spectrometry, Remote Sens. Environ., 113, 25–37, 2009.
Egli, L.: Spatial variability of new snow amounts derived from a dense network of Alpine automatic stations, Ann. Glaciol., 49, 51–55, 2008.
Egli, L.: Spatial variability of seasonal snow cover at different scales in the Swiss Alps, Ph.D. thesis, Diss. ETH No. 19658, Zürich, Switzerland, doi:10.3929/ethz-a-006689712, 2012.
Egli, L., Jonas, T. Grünewald T., Schirmer, T., and Burlando, P.: Dynamics of snow ablation in a small Alpine catchment observed by repeated terrestrial laser scans, Hydrol. Process., doi:10.1002/hyp.8244, 2011.
Elder, K., Dozier, J., and Michaelsen, J.: Snow accumulation and distribution in an alpine watershed, Water Resour. Res., 27, 1541–1552, 1991.
Elsasser, H. and Bürki, R.: Climate change as a threat to tourism in the Alps, Clim. Res., 20, 253–257, 2002.
Farinotti, D., Usselmann, S., Huss, M., Bauder, A., and Funk, M.: Runoff evolution in the Swiss Alps: projections for selected high-alpine catchments based on ENSEMBLES scenarios, Hydrol. Process., 26, 1909–1924, 2012.
Fily, M., Bourdelles, B., Dedieu, J. P., and Sergent, C.: Comparison of in situ and Landsat Thematic Mapper derived snow grain characteristics in the Alps, Remote Sens. Environ., 59, 452–460, 1997.
Fischer, L., Eisenbeiss, H., Kaab, A., Huggel, C., and Haeberli, W.: Monitoring topographic changes in a periglacial high-mountain face using high-resolution DTMs, Monte Rosa East Face, Italian Alps, Permafrost Periglac., 22, 140–152, 2011.
Foppa, N., Stoffel, A., and Meister, R.: Synergy of in situ and space borne observation for snow depth mapping in the Swiss Alps, Int. J. Appl. Earth Obs., 9, 294–310, 2007.
Frei, A., Tedesco, M., Lee, S., Foster, J., Hall, D. K., Kelly, R., and Robinson, D. A.: A review of global satellite-derived snow products, Adv. Space Res., 50, 1007–1029, 2012.
Grünewald, T., Schirmer, M., Mott, R., and Lehning, M.: Spatial and temporal variability of snow depth and ablation rates in a small mountain catchment, The Cryosphere, 4, 215–225, doi:10.5194/tc-4-215-2010, 2010.

Hall, D. K. and Martinec, J.: Remote sensing of ice and snow, Chapman and Hall Ltd., London, ISBN 0 421 25910, 189 pp., 1985.

Hall, D., Riggs, G., Salomonson, V., DiGirolamo, N., and Bayr, K.: MODIS snow-cover products, Remote Sens. Environ., 83, 181–194, 2002.

Höhle, J. and Höhle, M.: Accuracy assessment of digital elevation models by means of robust statistical methods, ISPRS J. Photogramm. Remote Sens., 64, 398–406, 2009.

Jonas, T., Marty, C., and Magnusson, J.: Estimating the snow water equivalent from snow depth measurements in the Swiss Alps, J. Hydrol., 378, 161–167, doi:10.1016/j.jhydrol.2009.09.021, 2010.

Koetz, B., Arino, O., Poulianen, J., and Bojkov, B.: GlobSnow – a new contribution to global snow monitoring services, edited by: Regner, P., MERIS and (A)ATSR workshop. Frascati, Italy, 2008.

Kraus, K.: Photogrammetrie, Walter de Gruyter GmbH, Berlin, 7, 516 pp., 2004.

Lehning, M., Löwe, H., Ryser, M., and Raderschall, N.: Inhomogeneous precipitation distribution and snow transport in steep terrain, Water Resour. Res., 44, W07404, 2008.

Lopez-Moreno, J. and Nogues-Bravo, D.: Interpolating local snow depth data: An evaluation of methods, Hydrol. Process., 20, 2217–2232, 2006.

Mancini, F., Dubbini, M., Gattelli, M., Stecchi, F., Fabbri, S., and Gabbianelli, G.: Using unmanned aerial vehicles (UAV) for high-resolution reconstruction of topography: the structure from motion approach on coastal environments, Remote Sens., 5, 6880–6898, 2013.

Melvold, K. and Skaugen, T.: Multiscale spatial variability of lidar-derived and modeled snow depth on Hardangervidda, Norway, Ann. Glaciol., 54, 273–281, 2013.

Nolin, A.: Recent advances in remote sensing of seasonal snow, J. Glaciol., 56, 1141–1150, 2011.

Nolin, A. W. and Dozier, J.: Estimating snow grain size using AVIRIS data, Remote Sens. Environ., 44, 231–238, 1993.

Nöthiger, C. and Elsasser, H.: Natural hazards and tourism: new findings on the European Alps, Mt. Res. Dev., 24, 24–27, 2004.

Painter, T. H., Roberts, D. A., Green, R. O., and Dozier, J.: The Effect of Grain Size on Spectral Mixture Analysis of Snow-Covered Area from AVIRIS Data, Remote Sens. Environ., 65, 320–332, 1996.

Prokop, A.: Assessing the applicability of terrestrial laser scanning for spatial snow depth measurements, Cold Reg. Sci. Technol., 54, 155–163, 2008.

Pulliainen, J.: Mapping of snow water equivalent and snow depth in boreal and sub-arctic zones by assimilating space-borne microwave radiometer data and ground-based observations, Remote Sens. Environ., 101, 257–269, 2006.
Rango, A. and Itten, K. I.: Satellite potentials in snowcover monitoring and runoff prediciton, Nord. Hydrol., 7, 209–230, 1976.
Rixen, C., Teich, M., Lardelli, C., Gallati, D., Pohl, M., Pütz, M., and Bebi, P.: Winter tourism and climate change in the Alps: an assessment of resource consumption, snow reliability, and future snowmaking potential, Mt. Res. Dev., 31, 229–236, 2011.
Rott, H.: Synthetic aperture radar capabilities for snow and glacier monitoring, Adv. Space Res., 4, 241–246, 1984.
Sandau, R. (Ed.): Digital Airborne Camera, Springer Netherlands, ISBN: 978-1-4020-8877-3 338 pp., 2012.
Sandmeier, J.: ReflexW software package, available at: http://www.sandmeier-geo.de/reflexw.html (last access: 21 April 2014), 2013.
Schanda, E., Matzler, C., and Kunzi, K.: Microwave remote sensing of snow cover, Int. J. Remote Sens., 4, 149–158, 1983.
Schweizer, J., Jamieson, J. B., and Schneebeli, M.: Snow avalanche formation, Rev. Geophys., 41, 2–25, 2003.
Schweizer, J., Kronholm, K., Jamieson, J. B., and Birkeland, K. W.: Review of spatial variability of snowpack properties and its importance for avalanche formation, Cold Reg. Sci. Technol., 51, 253–272, 2008.
Shi, J. and Dozier, J.: Estimation of snow water equivalence using SIR-C/X-SAR, II. Inferring snow depth and particle size, IEEE T. Geosci. Remote, 38, 2475–2488, 2000.
Swisstopo: Formeln und Konstanten für die Berechnung der Schweizerischen schiefachsigen Zylinderprojektion und der Transformation zwischen Koordinaten–systemen, Bundesamt für Landestopographie swisstopo, Bern, Switzerland, 2008.
Ulaby, F. and Stiles, W.: The active and passive microwave response to snow parameters, 2, Water equivalent of dry snow, J. Geophys. Res., 85, 1045–1049, 1980.
Veitinger, J., Sovilla, B., and Purves, R. S.: Influence of snow depth distribution on surface roughness in alpine terrain: a multi-scale approach, The Cryosphere, 8, 547–569, doi:10.5194/tc-8-547-2014, 2014.
Wipf, S., Stoeckli, V., and Bebi, P.: Winter climate change in alpine tundra: Plant responses to changes in snow depth and snowmelt timing, Climatic Change, 94, 105–12, 2009.

TCD
8, 3297–3333, 2014

Spatially continuous mapping of snow depth in high alpine catchments

Y. Bühler et al.

Title Page
Abstract Introduction
Conclusions References
Tables Figures
◂◂ ▸▸
◂ ▸
Back Close
Full Screen / Esc
Printer-friendly Version
Interactive Discussion

Zemp, M., Haeberli, W., Hoelzle, M., and Paul, F.: Alpine glaciers to disappear within decades?, Geophys. Res. Lett., 33, L13504, doi:10.1029/2006GL026319, 2006.
Zhang, B. and Miller, S. Adaptive automatic terrain extraction, Proc. SPIE 3072, P. Soc. Photo-Opt. Ins., 27, 926247, doi:10.1117/12.281065, 1997.

TCD
8, 3297–3333, 2014

Table 1. Statistical accuracy measures of error distributions ($DSM_{ADS} - DTM_{ALS}$) for 886 000 points in the test site Wannengrat (outlier removal: $\geq \mu \pm 3 \times$ RMSE).

μ	RMSE	$\mu*$	RMSE[a]	Median	NMAD
0.19	0.9	0.16	0.33	0.16	0.24

TCD
8, 3297–3333, 2014

TCD
8, 3297–3333, 2014

Spatially continuous mapping of snow depth in high alpine catchments

Y. Bühler et al.

Table 2. Correlated vs. interpolated terrain points in summer and winter DSM over the entire test site.

	correlated [n]	interpolated [n]	total [n]	correlated [%]
summer 2010	28 524 154	1 533 418	30 057 572	94.6
winter 2012	28 592 370	1 710 205	30 302 575	94.4

Table 3. ADS80 DSM derived snow depth values (4 by 4 pixels) compared to the hand measured snow depth values (5 by 5 single measurements) for the 15 plots. Plots where at least one measurement did not reach the ground are displayed in italic.

	min	max	mean	std	min ADS	max ADS	mean ADS	std ADS	Δ mean	Δ std
Plot 1	*1.80*	*3.10*	*2.81*	*0.42*	*1.68*	*3.41*	*2.56*	*0.55*	*0.25*	*−0.13*
Plot 2	0.85	2.50	1.43	0.53	0.52	2.16	1.25	0.52	0.18	0.01
Plot 3	1.20	1.75	1.43	0.16	0.90	1.72	1.14	0.15	0.29	0.01
Plot 4	0.35	0.90	0.50	0.15	0.30	0.59	0.43	0.09	0.07	0.06
Plot 5	0.55	1.75	1.01	0.34	0.04	1.84	0.79	0.53	0.22	−0.19
Plot 6	0.75	1.75	1.19	0.29	1.12	1.93	1.48	0.25	−0.29	0.04
Plot 7	1.35	2.90	2.32	0.47	1.98	2.69	2.34	0.21	−0.02	0.26
Plot 8	1.85	2.80	2.33	0.25	2.13	2.81	2.37	0.17	−0.04	0.08
Plot 9	1.40	2.20	1.71	0.23	1.43	2.04	1.69	0.17	0.02	0.06
Plot 10	0.55	2.35	1.34	0.56	0.77	2.14	1.40	0.38	−0.06	0.18
Plot 11	*0.65*	*3.10*	*2.28*	*0.67*	*0.56*	*2.65*	*1.93*	*0.85*	*0.35*	*−0.18*
Plot 12	0.15	0.35	0.22	0.06	0.06	0.24	0.14	0.05	0.08	0.01
Plot 13	*2.30*	*3.10*	*2.59*	*0.33*	*2.89*	*0.49*	*3.71*	*0.49*	*−1.12*	*−0.16*
Plot 14	0.70	2.00	1.37	0.41	0.43	1.62	1.12	0.32	0.25	0.09
Plot 15	0.35	1.60	0.97	0.33	0.75	1.81	1.33	0.27	−0.36	0.06

TCD
8, 3297–3333, 2014

Table 4. Overview on the accuracy measures calculated from the different reference datasets.

Reference dataset	No. of observations	RMSE	NAMD	$corr_e$
ALS (summer surface)	886 000	0.33	0.24	–
dGNSS (winter surface)	137	0.37	0.28	–
Hand plots (snow depth)	12	0.19	0.18	0.95
TLS (snow depth)	55 272	0.33	0.26	0.94
GPR (snow depth)	1522	0.43	0.37	0.45

TCD
8, 3297–3333, 2014

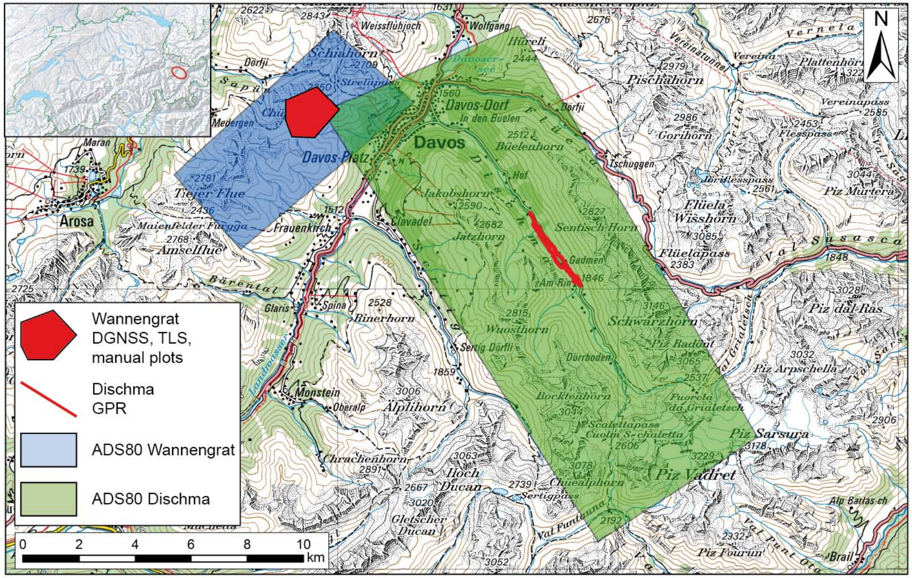

Figure 1. ADS80 data coverage and locations of the applied reference data sets at Wannengrat and in the Dischma valley close to Davos, Switzerland.
Pixmap ©2014 swisstopo (5704 000 000).

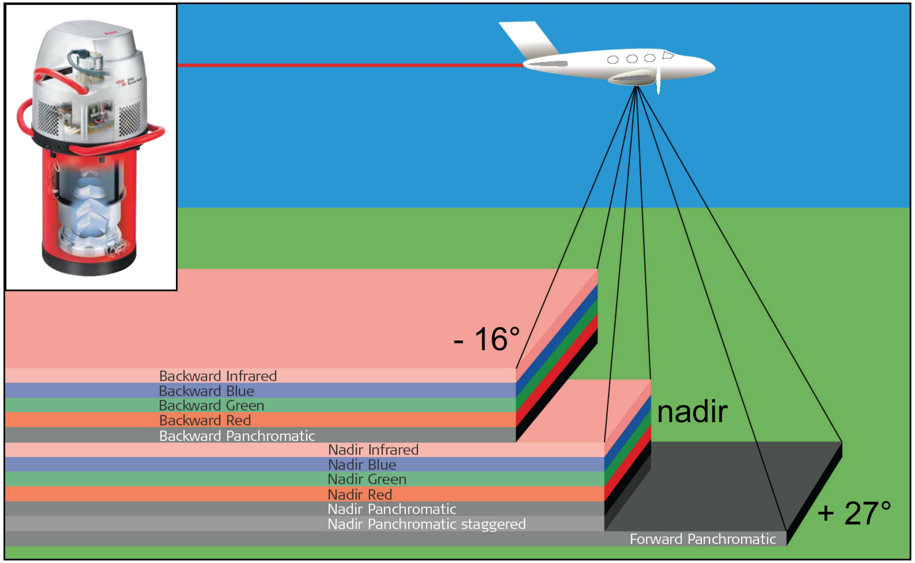

Figure 2. ADS 80 sensor (top left) and data acquisition scheme with spectral bands and viewing angles (Bühler et al., 2009).

TCD
8, 3297–3333, 2014

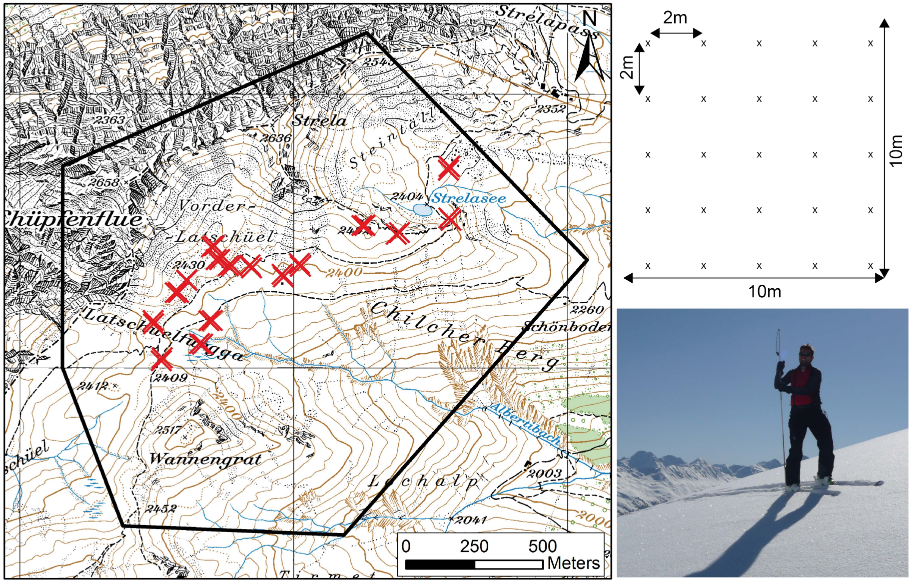

Figure 3. Location of the plots measured by hand and applied sampling strategy. Pixmap ©2014 swisstopo (5704 000 000).

TCD
8, 3297–3333, 2014
Spatially continuous mapping of snow depth in high alpine catchments
Y. Bühler et al.

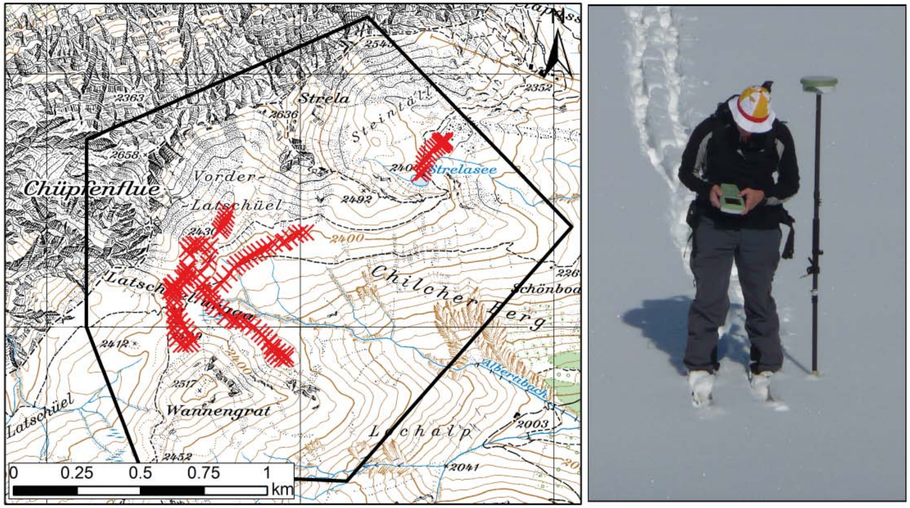

Figure 4. Location of the 137 dGNSS measurements (left) and a photography of the device at the day of data acquisition (right).

TCD
8, 3297–3333, 2014

Spatially continuous mapping of snow depth in high alpine catchments

Y. Bühler et al.

Figure 5. View of the TLS test site from the scanner position towards Strela and Kilcherberg (SW) on 20 March 2012.

TCD
8, 3297–3333, 2014

Spatially continuous mapping of snow depth in high alpine catchments

Y. Bühler et al.

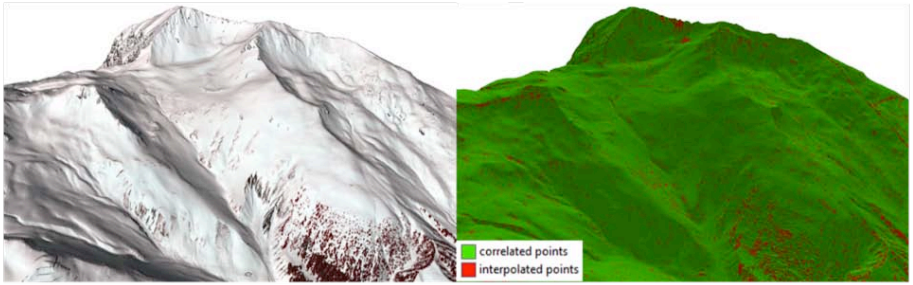

Figure 6. Spatial distribution of image correlation success in a section of the test site Wannengrat. Visible in the right picture are interpolated points (red) mainly in very steep terrain (> 50°), on vegetation and anthropogenic features (e.g. ski lift).

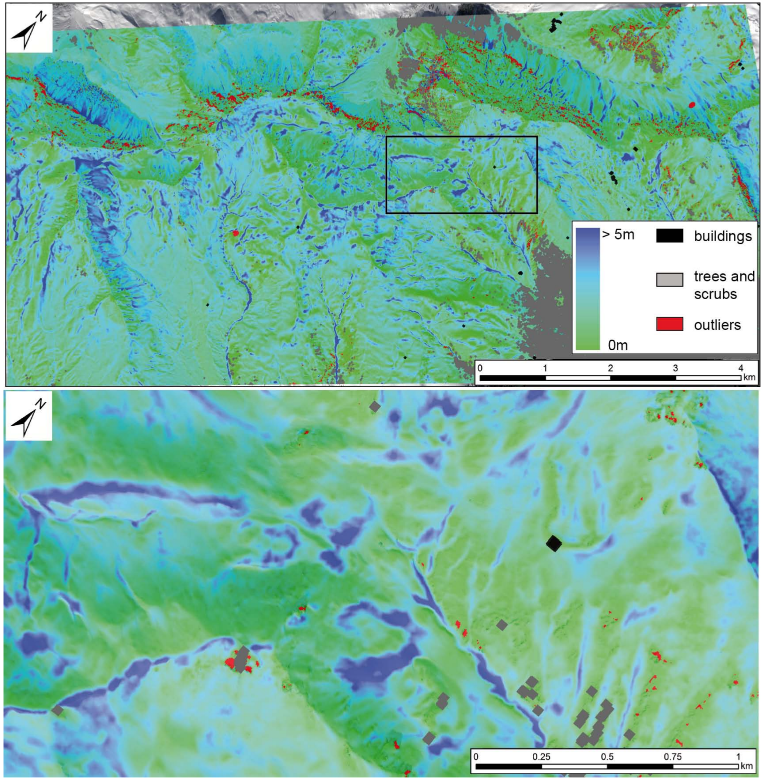

Figure 7. Snow depth map of the entire Wannengrat area (top, see Fig. 1. for orientation) and a close up view from area where the reference data was acquired (bottom). Traps for wind-blown snow, cornices and deposits from past avalanche events can be identified by the highest snow depth values.

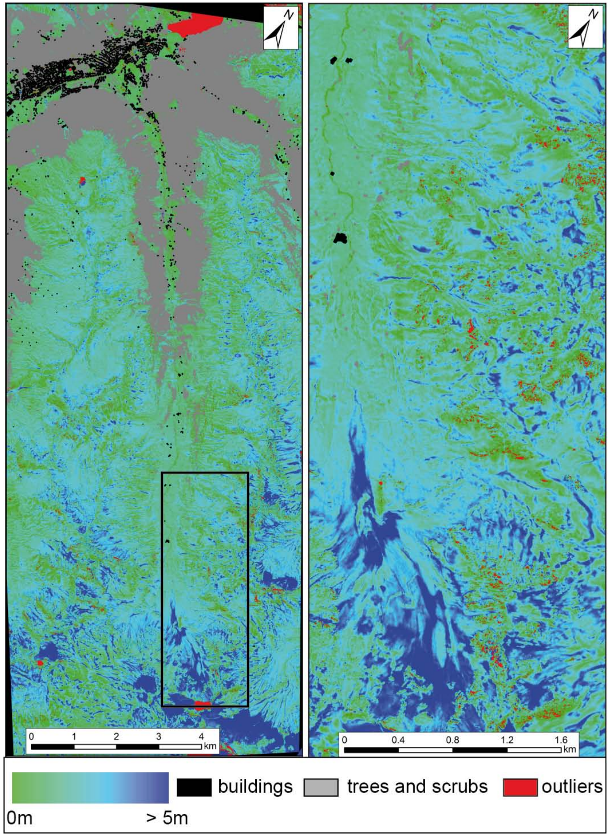

Figure 8. Snow depth map of the entire Dischma area (left, see Fig. 1. for orientation) and a close up view (right) from area indicated by the black box.

TCD
8, 3297–3333, 2014

Spatially continuous mapping of snow depth in high alpine catchments

Y. Bühler et al.

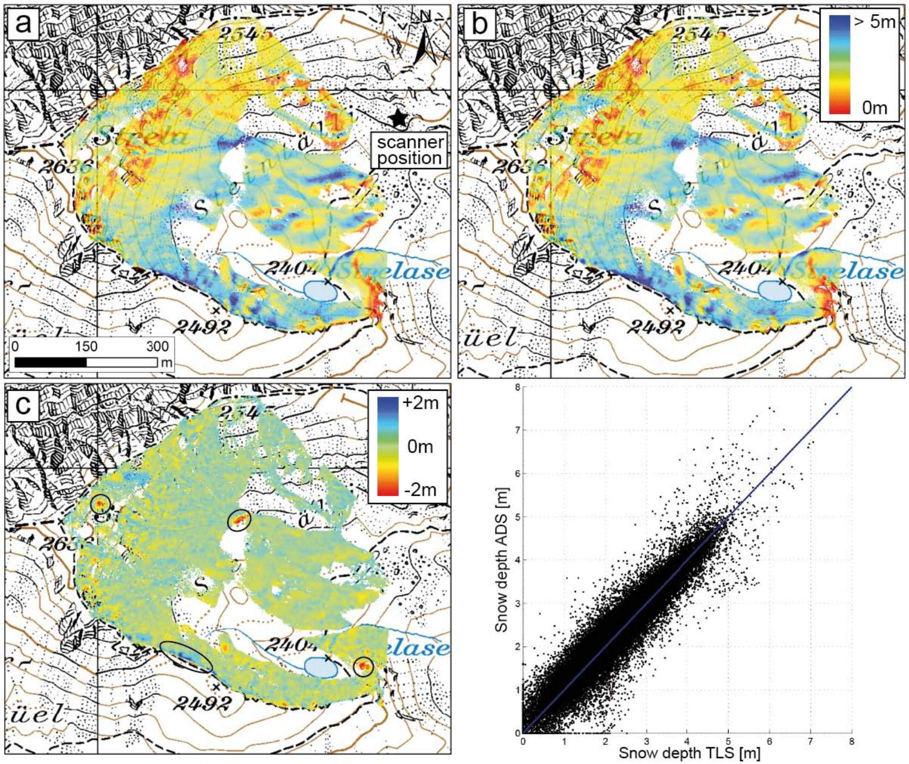

Figure 9. TLS derived snow depth **(a)**, ADS80 derived snow depth **(b)**, difference ADS minus TLS **(c)** and the correlation between the two different snow depth measurements ($cor_e = 0.94$).

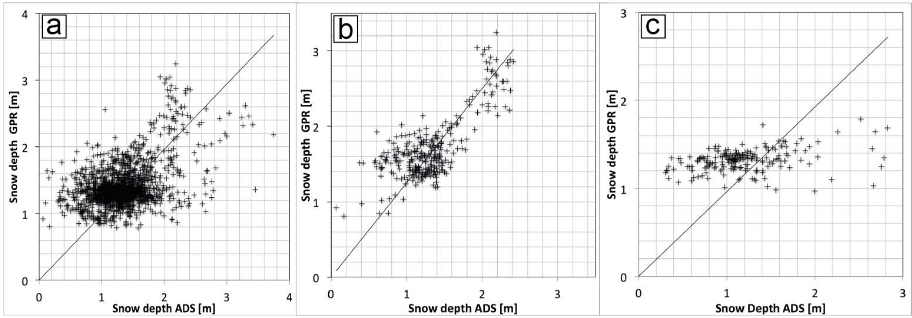

Figure 10. Correlation of the ADS snow depth to the GPR snow depth for all 1522 points (**a**, $cor_e = 0.45$), segment No. 1 with 296 points and a larger value range (**b**, $cor_e = 0.77$) and segments No. 5 with 191 points and a low value range in the GPR data (**c**, $cor_e = 0.34$).

TCD
8, 3297–3333, 2014

Spatially continuous mapping of snow depth in high alpine catchments

Y. Bühler et al.